Sum Frequency Generation Vibrational Spectroscopy of Colloidal Platinum Nanoparticle Catalysts: Disordering versus Removal of Organic Capping

James M. Krier,[†,‡] William D. Michalak,[†,‡] L. Robert Baker,*[,†,‡] Kwangjin An,[†,‡] Kyriakos Komvopoulos,[§] and Gabor A. Somorjai*[,†,‡]

[†]Department of Chemistry, University of California, Berkeley, California 94720, United States

[‡]Materials Sciences and Chemical Sciences Divisions, Lawrence Berkeley National Laboratory, Berkeley, California 94720, United States

[§]Department of Mechanical Engineering, University of California, Berkeley, California 94720, United States

ABSTRACT: Recent work with nanoparticle catalysts shows that size and shape control on the nanometer scale influences reaction rate and selectivity. Sum frequency generation (SFG) vibrational spectroscopy is a powerful tool for studying heterogeneous catalysis because it enables the observation of surface intermediates during catalytic reactions. To control the size and shape of catalytic nanoparticles, an organic ligand was used as a capping agent to stabilize nanoparticles during synthesis. However, the presence of an organic capping agent presents two major challenges in SFG and catalytic reaction studies: it blocks a significant fraction of active surface sites and produces a strong signal that prevents the detection of reaction intermediates with SFG. Two methods for cleaning Pt nanoparticles capped with poly(vinylpyrrolidone) (PVP) are examined in this study: solvent cleaning and UV cleaning. Solvent cleaning leaves more PVP intact and relies on disordering with hydrogen gas to reduce the SFG signal of PVP. In contrast, UV cleaning depends on nearly complete removal of PVP to reduce SFG signal. Both UV and solvent cleaning enable the detection of reaction intermediates by SFG. However, solvent cleaning also yields nanoparticles that are stable under reaction conditions, whereas UV cleaning results in aggregation during reaction. The results of this study indicate that solvent cleaning is more advantageous for studying the effects of nanoparticle size and shape on catalytic selectivity by SFG vibrational spectroscopy.
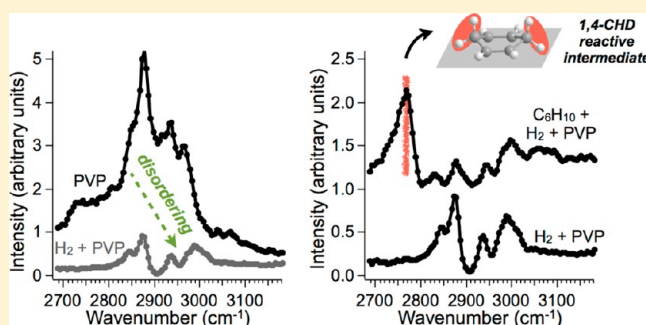
1. INTRODUCTION

Sum frequency generation (SFG)[1,2] vibrational spectroscopy is a second-order optical process that measures the vibrational spectrum of molecules on a surface or an interface. This technique is a powerful tool for studying heterogeneous catalysis because it enables the observation of surface intermediates during catalytic reactions. SFG vibrational spectroscopy has been used to study reactions on both single-crystal catalysts[3−5] and 2D films of nanoparticle catalysts.[6,7] Recent work on nanoparticle catalysts has shown that size and shape control on the nanometer scale is critical for reaction selectivity.[8−12] This is a major advance for heterogeneous catalysis and motivates the present effort to observe reaction intermediates on size- and shape-controlled nanoparticles under reaction conditions.

A major challenge in the detection of reaction intermediates is the background of molecular stretches originating from the organic capping layer of colloidal nanoparticles. Nanoparticles require a layer of organic ligands to stabilize both size and shape. However, the organic capping layer has two major effects on catalytic reaction studies. First, it blocks active sites on the

nanoparticles reducing catalytic activity. Second, it produces a strong signal in the SFG spectrum, making the observation of reaction intermediates on the nanoparticles difficult or impossible. Common capping agents, including poly(vinylpyrrolidone) (PVP),[13] cetyltrimethylammonium bromide (CTAB),[14] tetradecyltrimethylammonium bromide (TTAB),[15] hexadecylamine (HDA),[16] and oleylamine[17] produce a signal in the aliphatic range, preventing the identification of C−H vibrations of reactive catalytic intermediates.

UV light has been previously used to remove the organic capping agent from nanoparticles.[7,18,19] This study compares UV cleaning of nanoparticles (often called "UVO" or "UV-ozone") and a simpler, yet more effective method, termed solvent cleaning, which removes excess capping (PVP) from the nanoparticles. It is shown that both UV and solvent cleaning of Pt nanoparticles enable the observation of reaction intermediates by SFG spectroscopy. However, solvent cleaning

leaves more PVP intact and relies on disordering under hydrogen to reduce its SFG signal, whereas UV cleaning reduces the signal from PVP by nearly complete removal. It is also shown that solvent cleaning produces nanoparticles that are stable under reaction conditions, whereas UV cleaning results in nanoparticle aggregation during reaction. Therefore, solvent cleaning makes it possible to study size- and shape-dependent nanoparticle selectivity using SFG vibrational spectroscopy.

Cyclohexene (C_6H_{10}) hydrogenation is a good reaction for SFG analysis because it produces intermediates with unique and well-documented[5,20−25] vibrational signatures. Three different reaction intermediates of cyclohexene hydrogenation exist on Pt that are easily identifiable in the SFG spectrum: 1,4-cyclohexadiene (1,4-CHD), 1,3-cyclohexadiene (1,3-CHD), and π-allyl. The spectrum of 1,4-CHD has a single peak at 2765 cm^{-1}, corresponding to a strongly red-shifted CH_2 asymmetric stretch. 1,3-CHD has three CH_2 stretches at 2830, 2875, and 2900 cm^{-1}, whereas the π-allyl has a strong CH_2 asymmetric stretch at 2920 cm^{-1} and a weak symmetric CH_2 stretch at 2840 cm^{-1}. Using cyclohexene hydrogenation on Pt as a model reaction, the catalytic activity and vibrational spectra of solvent-cleaned Pt nanoparticles were examined under reaction conditions and compared with those of UV-cleaned Pt nanoparticles.

2. EXPERIMENTAL METHODS

2.1. Nanoparticle Synthesis. Pt particles of 4.2 nm average size were synthesized using 100 mg chloroplatinic acid hexahydrate ($H_2Pt(IV)Cl_6 \cdot 6H_2O$, 37.5% metal basis, Sigma-Aldrich), 440 mg PVP (29 K, Sigma-Aldrich), and 20 mL of ethylene glycol (ReagentPlus, Sigma-Aldrich). The mixture was combined in a 25 mL round-bottomed flask, pumped to remove air, and flushed with Ar. The flask was then placed in an oil bath at 165 °C for 1 h under Ar flow.

Pt nanoparticles of 3.0 nm average size[26] were synthesized using 40 mg ammonium tetrachloroplatinate(II) (($NH_4)_2Pt$-$(II)Cl_4$), 220 mg PVP (29 K, Sigma-Aldrich), and 20 mL of ethylene glycol (ReagentPlus, Sigma-Aldrich). The mixture was combined in a 25 mL round-bottomed flask, pumped to remove air, and flushed with Ar. The flask was then placed in an oil bath at 165 °C for 30 min under Ar flow.

Pt nanoparticles of 1.7 nm average size[27] were synthesized by combining 250 mg chloroplatinic acid hexahydrate ($H_2Pt(IV)$-$Cl_6 \cdot 6H_2O$, 37.5% metal basis, Sigma-Aldrich), 25 mL of ethylene glycol (ReagentPlus, Sigma-Aldrich), and 0.00625 g NaOH under Ar at 433 K for 1 h. After synthesis, the nanoparticles were precipitated with 1.0 M HCl and then combined with PVP.

Nanoparticles of different sizes were separated from the ethylene glycol synthesis mixture by precipitation with acetone and centrifugation at 4000 rpm for 5 min. Then, the nanoparticles were dissolved by sonication in 20 mL of ethanol, mixed with 25 mL of hexane, and centrifuged again for precipitation. This process was repeated three times to remove ethylene glycol and excess chloroplatinic acid from the synthesis. Hereafter, these nanoparticles will be referred to as fully-capped nanoparticles.

2.2. Solvent Cleaning. For the 4.2 and 3.0 nm nanoparticles, solvent cleaning consisted of five additional cycles of ethanol washing, followed by precipitation in hexane for a total of eight ethanol washes after synthesis. Following these cycles of ethanol washing, the nanoparticles were further washed two

times, once in chloroform and once in isopropyl alcohol. Because the 1.7 nm nanoparticles retained less PVP, they did not require as many washing cycles. Therefore, these nanoparticles were washed only one additional time in ethanol for a total of four ethanol washes after synthesis. If washed more times, 1.7 nm nanoparticles aggregate in solution.

2.3. Langmuir−Blodgett Film Deposition. Nanoparticles were first dissolved in a 50/50 ethanol/chloroform mixture and then deposited onto a water surface.[28] For Langmuir−Blodgett (LB) deposition, a suspension of nanoparticles in the ethanol/chloroform mixture was dispersed onto a water surface. Sufficient time was allowed for the organic solvent to evaporate, leaving a 2D dispersion of nanoparticles on water. The film was then compressed, and the increase in surface pressure was monitored. When the desired surface pressure was reached, the SFG prism was pulled through the water at a rate of 3 mm/min, and a monolayer film of nanoparticles was deposited onto the prism surface. For SFG experiments, a surface pressure of 20 mN/m was used for LB films. Film deposition on transmission electron microscopy (TEM) grids was accomplished by dropping the grid on the compressed LB film for 10 s and then retrieving the grid with tweezers. For TEM experiments, a surface pressure of 8 mN/m was used to obtain nanoparticle films of low density. This provided better visibility of nanoparticle aggregation that occurred for some samples under reaction conditions. The Nima 611 LB trough with filter paper as the surface tension probe was used in all film depositions.

2.4. UV Cleaning. Two low-pressure mercury lamps (Lights Sources, model number GPH357T5VH/4P) were used for UV treatment inside a clean aluminum box. Samples were placed 5 mm below one lamp and exposed to 254 and 185 nm irradiation for a specified time.

2.5. Sum Frequency Generation Vibrational Spectroscopy. A mode-locked Nd:YAG dye laser (Continuum D-20) with 1064 nm fundamental output, 20 Hz repetition rate, and 20 ps pulse width was used in all of the experiments described herein. A frequency-doubling crystal was used to generate a visible (532 nm) beam from the fundamental beam. An optical parametric generator/amplifier produced tunable infrared in the range 2680−3180 cm^{-1}, corresponding to the stretching modes of aliphatic and aromatic groups. Visible and infrared beams of 130 μJ power were spatially and temporally overlapped at the base of the SFG prism at angles of 63 and 48°, respectively, from the surface normal to achieve total internal reflection (Figure 1). All of the experiments were performed in *ppp* polarization combination. Polished fused silica equilateral (60°) prisms (ISP Optics) were used in all experiments. A photomultiplier tube with a gated boxcar integrator detected SFG photons. Each LB nanoparticle film was probed with SFG under 1 atm of total pressure.

The SFG signal intensity I_{SFG} can be understood in terms of the second-order nonlinear susceptibility constant $\chi^{(2)}$:

$$I_{SFG} \propto |\chi_{NR}^{(2)} + \chi_{R}^{(2)}|^2 = \left| \chi_{NR}^{(2)} + \frac{A_q}{\omega_{IR} - \omega_q + i\Gamma} \right|^2$$

with

$$A_{q,ijk} = N_S \sum_{lmn} a_{q,lmn} \langle (\hat{i} \cdot \hat{l})(\hat{j} \cdot \hat{m})(\hat{k} \cdot \hat{n}) \rangle$$

where $\chi_{NR}^{(2)}$, $\chi_{R}^{(2)}$, A_q, ω_{IR}, ω_q, and Γ are nonresonant[30] contributions, resonant contributions, amplitude, infrared
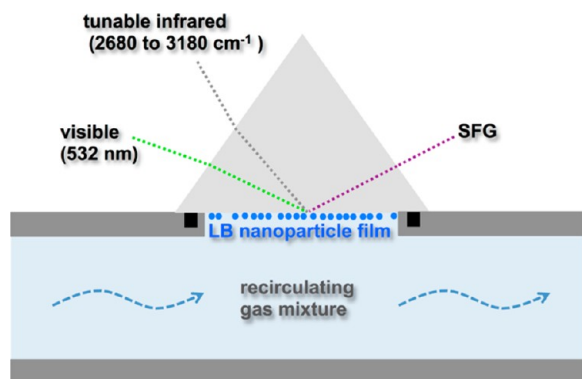
Figure 1. Schematic of SFG experiment with LB nanoparticle films deposited on a silica prism. Gas mixtures (Ar, H_2/Ar, and C_6H_{10}/H_2/Ar) are flowed over the sample while SFG spectra are recorded.

Figure 2. SFG spectra of fully-capped 4.2 nm Pt-PVP nanoparticles obtained at 298 K in different atmospheres: (A) 760 Torr Ar (top) and 200 Torr H_2, 560 Torr Ar (bottom) and (B) 10 Torr C_6H_{10}, 200 Torr H_2, 550 Torr Ar (top) and 200 Torr H_2, 560 Torr Ar (bottom). Spectra shown in (B) are offset for clarity. Unlabeled features are attributed to PVP.

Figure 3. SFG spectra of solvent-cleaned 4.2 nm Pt-PVP nanoparticles obtained at 298 K in different atmospheres: (A) 760 Torr Ar (top) and 200 Torr H_2, 560 Torr Ar (bottom) and (B) 10 Torr C_6H_{10}, 200 Torr H_2, 550 Torr Ar (top) and 200 Torr H_2, 560 Torr Ar (bottom). Spectra shown in (B) are offset for clarity. Unlabeled features are attributed to PVP.

frequency, *qth* mode frequency, and damping factor, respectively. Oscillator strength A_q reflects the number density N_S, Raman/infrared response a_q, and average oscillator orientation $\langle \cdot \cdot \rangle$ (encompassing both lab coordinates *ijk* and molecular coordinates *lmn*). Unlike the varied forms of linear vibrational spectroscopy, SFG requires a net orientation along the *z* axis (perpendicular to the surface), which gives surface selectivity. This indicates that even concentrated vibrational modes will ultimately cancel if present only in random disordered directions.

2.6. Transmission Electron Microscopy. TEM images of LB films were obtained with a JEOL 2100 microscope operated at 200 kV. Silicone (SiO) films on copper grids (Electron Microscopy Sciences) were used as substrates for all TEM images presented here.

2.7. Kinetic Measurements. Turnover rates were measured with a Hewlett-Packard 5890 Series II gas chromatograph connected to a circulating batch reactor. The Restek Haysep Q 80/100 column was used to measure ethylene hydrogenation rate, and the Alltech AT-1000 column was used to measure cyclohexene hydrogenation rate.

3. RESULTS AND DISCUSSION

3.1. Effect of PVP Removal on Detection of Reaction Intermediates on Pt Nanoparticles. The capping agent presents a challenge for SFG studies of colloidal nanoparticle catalysts because its signal often overlaps with that of the reactive intermediate of interest and also blocks catalytically active surface sites. In the presence of H_2, PVP becomes disordered on fully-capped nanoparticles, as shown by the significant decrease in background signal intensity (Figure 2A). However, even in the absence of a background signal from the PVP, a signal from the reaction intermediate (1,4-CHD) cannot be easily observed during cyclohexene hydrogenation (Figure 2B) because of site blocking by disordered PVP.

In the case of solvent-cleaned nanoparticles, a strong signal from PVP is still observed in the SFG spectrum (Figure 3A). This is because solvent cleaning does not remove all PVP; if it did, then the nanoparticles would aggregate in solution. Similar to fully-capped nanoparticles (Figure 2A), the signal from PVP diminishes in H_2 due to the disordering effect (Figure 3A). However, the major difference between fully-capped and solvent-cleaned nanoparticles can be observed by comparing the spectra obtained under reaction conditions (Figures 2B and 3B). Under cyclohexene hydrogenation conditions, the 1,4-
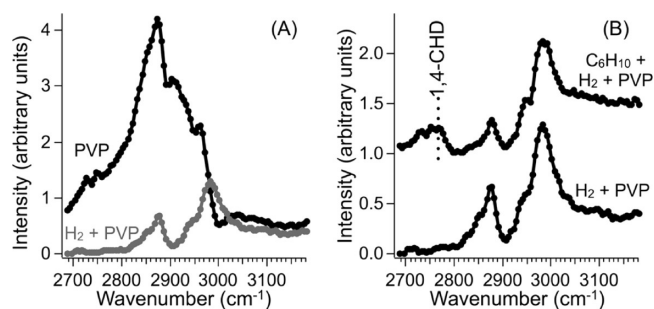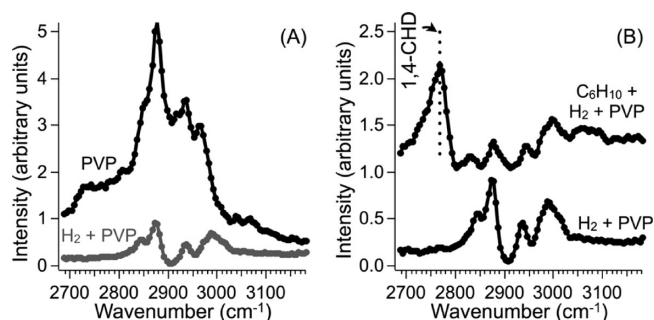
CHD intermediate is clearly visible in the SFG spectrum of the solvent-cleaned Pt nanoparticles (Figure 3B), indicating significant adsorption on the Pt nanoparticle surface. This finding indicates that although the solvent-cleaned nanoparticles are lightly capped with PVP, there are sufficient Pt sites available for catalysis and for observing reaction intermediates with SFG.

Because the peak of 1,4-CHD occurs at a unique wavenumber position compared to other aliphatic vibrations, it is certain that it arises from a chemisorbed reaction intermediate on the surface of the Pt nanoparticle and not from PVP. Interestingly, when cyclohexene is introduced with H_2, the remaining PVP peaks are further suppressed from the level observed with only H_2. This suggests that 1,4-CHD displaces PVP from the Pt surface into a disordered geometry. SFG spectra were also collected during cyclohexene hydrogenation on 1.7 and 3.0 nm Pt nanoparticles. These spectra (not shown here) also indicate a strong peak corresponding to the 1,4-CHD intermediate. The 1.7 nm Pt nanoparticles retain less PVP than larger nanoparticles and do not require as much solvent cleaning for observing surface intermediates. (See Section 2.2.)

Although the role of solvent cleaning to increase the available Pt surface area through PVP removal is intuitive, the role of H_2 to decrease the background signal of PVP is less obvious and needs further interpretation. H_2 dramatically reduces the signal from PVP on both fully-capped and solvent-cleaned nano-

particles (Figures 2A and 3A). Under an inert atmosphere of Ar gas, the full signal of PVP capping is strong for both types of nanoparticles. However, adding H_2 reduces the signal of PVP to relatively weak peaks located at 2850 (symmetric CH_2, chain), 2870 (symmetric CH_2, chain), 2930 (asymmetric CH_2, chain), and 2980 cm^{-1} (asymmetric CH_2, ring).[31]

SFG selection rules indicate that decreasing concentration or increasing disorder reduce signal. Although the effect of concentration on the spectral intensity is expected, it is important to recognize the effect of molecular ordering on the spectral intensity. Because SFG vibrational spectroscopy is a coherent process, it is not only sensitive to individual molecular susceptibilities but also to the net susceptibility of the ensemble of molecular oscillators. Consequently, if molecules on a surface are highly disordered, then the net ensemble will not produce a strong SFG signal, even if the concentration is high.

The following two examples emphasize this concept. In a recent study,[32] the ordering of mixed self-assembled monolayers of fluorinated alkyl phosphonic acid and C_{60} functionalized octadecyl phosphonic acid was tuned by varying the amounts of each component. For certain mixtures, the SFG intensity from C_{60} molecules decreased even as its surface density increased. This effect is attributed to disordering of the self-assembled monolayer. In another case,[5] the observed peaks from the π-allyl intermediate on Pt(111) increased in intensity by eight-fold when the pressure was changed from ambient to ultrahigh vacuum. Because the surface concentration did not increase dramatically in vacuum relative to ambient pressure, the increased ordering strongly contributed to the signal enhancement. Therefore, it may be concluded that the addition of H_2 disorders PVP on Pt, as indicated by the decrease in SFG signal intensity by ~90%. This spectral change is reversible — when the cell is evacuated to vacuum, the full signal of PVP reappears. Disordering likely arises because of a weakened interaction between PVP and Pt. Several previous studies[11,33,34] report lower adsorption energies of organic molecules on Pt in the presence of H_2.

UV light of 254 and 185 nm wavelength is known to photodecompose organic materials, including PVP, through photolysis and ozonolysis mechanisms.[35] Accordingly, UV cleaning has been proposed[18] as a viable method for removing PVP from Pt nanoparticles. However, the effects of UV cleaning on the catalytic behavior of Pt nanoparticles are not fully understood.

Figure 4 shows SFG spectra of PVP-capped Pt nanoparticles after 180 min of UV exposure. The spectrum of the Pt nanoparticles in Ar (Figure 4A) shows a significant signal reduction in the aliphatic range compared to fully-capped and solvent-cleaned nanoparticles under the same conditions. This is attributed to the photodecomposition of PVP by UV light. Supporting evidence of PVP removal by UV cleaning was obtained from XPS analysis. It was found that the C content relative to Pt decreases by at least 90% after 10 min of UV cleaning. However, when the UV-cleaned nanoparticles are exposed to H_2, the signal in the aliphatic range increases significantly (Figure 4A), suggesting that although UV cleaning removes the majority of PVP, a C shell remains ("residual PVP") that subsequently reacts with H_2. This observation highlights the difficulty of preparing atomically clean Pt nanoparticles by UV cleaning. Further studies are in progress to probe the effect of the C shell on Pt catalysis. However, the shell does not prevent adsorption of cyclohexene — 1,4-CHD, 1,3-CHD, and π-allyl intermediates are readily observed on the
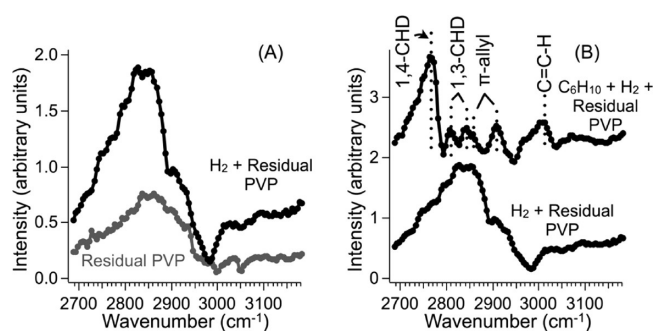

Figure 4. SFG spectra of UV-cleaned (180 min) 4.2 nm Pt-PVP nanoparticles obtained at 298 K in different atmospheres: (A) 760 Torr Ar (bottom) and 200 Torr H_2, 560 Torr Ar (top) and (B) 10 Torr C_6H_{10}, 200 Torr H_2, 550 Torr Ar (top) and 200 Torr H_2, 560 Torr Ar (bottom). Spectra shown in (B) are offset for clarity. Unlabeled features are attributed to PVP.

UV-cleaned nanoparticles under reaction conditions (Figure 4B).

Figure 5A shows SFG spectra of 4.2 nm Pt nanoparticles during cyclohexene hydrogenation at 298 K versus UV cleaning time. The removal of PVP is confirmed by the change in C/Pt atomic ratio (obtained by XPS) versus UV cleaning time shown in Figure 5B. As expected, the signal from cyclohexene hydrogenation intermediates steadily increases with UV treatment, indicating increased coverage by reactants. This is
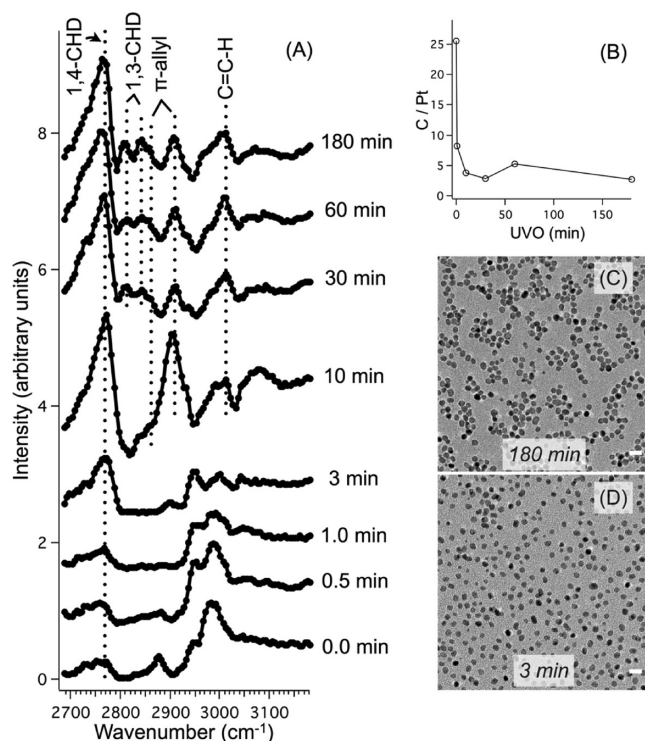

Figure 5. (A) SFG spectra of 4.2 nm Pt-PVP nanoparticles obtained at 298 K after UV cleaning (0 to 180 min) under cyclohexene hydrogenation reaction conditions (10 Torr C_6H_{10}, 200 Torr H_2, 550 Torr Ar). The observed intermediates change from exclusively 1,4-CHD (0–3 min) to 1,4-CHD, 1,3-CHD, and π-allyl (30–180 min). (B) XPS results showing the C/Pt ratio as a function of UV exposure time. (C,D) TEM images of UV-cleaned 4.2 nm Pt nanoparticles showing clustering after long treatment (180 min) but no aggregation (scale bar = 10 nm).
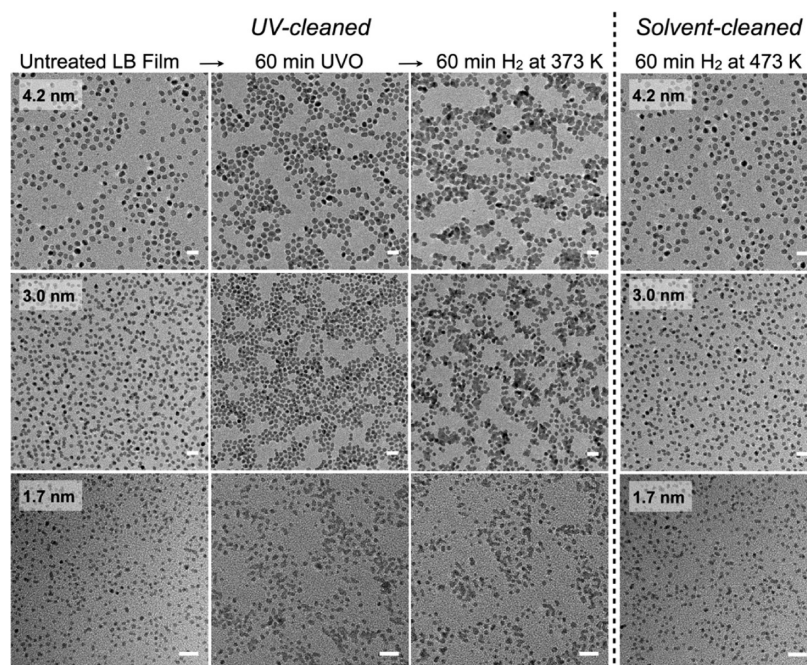
Figure 6. TEM images (scale bar = 10 nm) showing UV-cleaned and solvent-cleaned Pt-PVP nanoparticles under reaction conditions. For 4.2 and 3.0 nm nanoparticles, 60 min of UV treatment resulted in clustering, with neighboring nanoparticles moving closer to each other while maintaining their size. Under hydrogenation reaction conditions (200 Torr H_2, 560 Torr Ar, 373 K), clustered nanoparticles often melted together to produce much larger particles. Spherical 1.7 nm nanoparticles aggregated after 60 min of UV treatment. In contrast, under hydrogenation reaction conditions (200 Torr H_2, 560 Torr Ar) solvent-cleaned Pt-PVP nanoparticles did not exhibit changes up to at least 473 K.

most obvious for the 1,4-CHD intermediate (2765 cm^{-1}). Further changes in the SFG spectrum occurred with increasing UV cleaning time. UV treatment up to 3 min indicated the formation of only 1,4-CHD, which is consistent with the spectrum of solvent-cleaned nanoparticles (Figure 3B). However, longer UV treatment (10 min) produced an intense new peak at 2900 cm^{-1} with a weak counterpart at 2850 cm^{-1}, both assigned to π-allyl. For UV cleaning times ranging from 30 to 180 min, the π-allyl signal decreases, and new peaks appear (2810 and 2845 cm^{-1}), indicating 1,3-CHD. To observe each of these three intermediates on the Pt(111) single crystal with a comparable cyclohexene/H_2 ratio, the temperature must be increased from 303 to 483 K.[24] In this case, all three intermediates are observed at 298 K on 4.2 nm Pt by removing PVP.

The morphological stability of 4.2 nm nanoparticles during UV cleaning at 298 K is demonstrated by TEM images shown in Figure 5. Although long UV treatment (180 min) causes nanoparticle clustering (Figure 5C), aggregation does not occur — the nanoparticle size and shape is similar to that observed after 3 min of UV cleaning (Figure 5D). Consequently, changes in observed intermediates cannot be attributed to nanoparticle size or shape effects. Interestingly, the 1,3-CHD intermediate is much more active for cyclohexene hydrogenation on Pt(111) than the 1,4-CHD intermediate.[24] Therefore, it may be inferred that 180 min of UV cleaning produces nanoparticles that are more catalytically active than the fully-capped nanoparticles because the 1,3-CHD intermediate is observed only after extensive UV cleaning. Kinetic experiments of the present study show that the UV-cleaned catalyst is approximately three times more active for cyclohexene hydrogenation than the fully-capped catalyst, even after correcting for the number of Pt active sites (counted with ethylene hydrogenation). These spectral changes correlate with reaction kinetics and suggest

that besides simply blocking equivalent Pt sites, the capping agent may actively promote or inhibit the formation of certain reaction intermediates. Considering the capping agent as an active, dynamic support for nanoparticle catalysis is an intriguing concept that will be investigated in future studies.

3.2. Effect of Solvent Cleaning on Size Monodispersity of Pt Nanoparticles During Reaction. The stability of Pt nanoparticles under reaction conditions after solvent cleaning or UV cleaning can be assessed in the light of TEM results presented in this section. Figure 6 shows TEM images of fully-capped Pt nanoparticles of three sizes (4.2, 3.0, and 1.7 nm) as LB films before and after two treatments (60 min of UV cleaning, followed by 60 min under hydrogenation reaction conditions). Although 60 min of UV cleaning caused 4.2 and 3.0 nm nanoparticles to cluster closely together, these nanoparticles maintained a monodisperse size distribution. However, exposure to H_2 at 373 K resulted in melting and loss of size monodispersity. 1.7 nm Pt nanoparticles are even less stable and melted after UV cleaning, even before exposure to elevated temperature. Although the images shown in Figure 6 were obtained with silicone TEM grids, the same phenomena were observed with several other supports, including SiO_2 and TiO_2.

Figure 6 also shows TEM images demonstrating the stability of solvent-cleaned Pt nanoparticles. These images show solvent-cleaned nanoparticles of 4.2, 3.0, and 1.7 nm sizes after H_2 exposure at 473 K (i.e., 100 K higher temperature than that applied to UV-cleaned nanoparticles). It is clear that solvent-cleaned nanoparticles are very stable because they appear the same as the untreated LB film. This represents the major advantage of solvent cleaning compared to UV cleaning. Although UV cleaning is effective in removing PVP, it compromises nanoparticle stability under reaction conditions, resulting in the loss of size monodispersity. Alternatively,

solvent cleaning produces stable nanoparticle catalysts that allow for nanoscale size effects of selectivity to be studied by SFG vibrational spectroscopy.

3.3. Effect of Solvent and UV Cleaning on Number Density of Pt Active Sites. The role of solvent and UV cleaning on the number of available active sites of Pt nanoparticles was examined with ethylene hydrogenation experiments performed at 298 K. Ethylene hydrogenation on Pt is a structure insensitive reaction with a well-characterized turnover frequency.[26] Accordingly, the activity of a catalyst for ethane production from ethylene can be used to determine the number of active Pt sites on the catalyst.

Figure 7 shows the number density of active sites for fully-capped, solvent-cleaned, and UV-cleaned 4.2 nm Pt-PVP films.
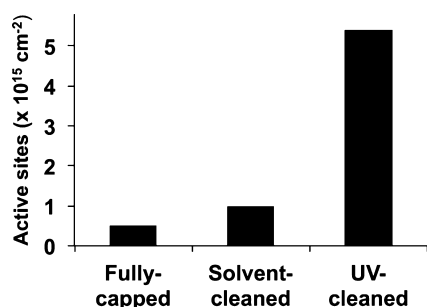

Figure 7. Active sites on layers of fully-capped, solvent-cleaned, and UV-cleaned 4.2 nm Pt nanoparticles with PVP capping agent determined from ethylene hydrogenation.

Surface coverage of the nanoparticles was controlled by the surface pressure applied during LB film deposition and should not vary significantly among samples. For a surface pressure of 20 mN/m, surface coverage by the nanoparticles was found to be 30−50%. Assuming 4.2 nm spherical nanoparticles with a (111) surface and no poisoning by the PVP capping agent, this surface coverage implies $\sim 2 \times 10^{15}$ Pt sites per cm^2.

Fully-capped nanoparticles contain 5×10^{14} active Pt sites per cm^2, as determined from ethylene hydrogenation measurements, representing $\sim 20\%$ of the apparent area. UV-cleaned nanoparticle LB films demonstrate higher densities of active sites by about an order of magnitude. Using ethylene hydrogenation measurements, the number densities of active sites on solvent- and UV-cleaned nanoparticle films are estimated to be 1×10^{15} and 4×10^{15} active sites per cm^2, corresponding to 40 and >100% of the apparent area, respectively. The higher activity of the UV-cleaned nanoparticles is attributed to a deviation of the actual number of active sites per nanoparticle from what is expected by assuming a sphere with a perfect (111) surface. However, this comparison is still insightful and shows that although solvent cleaning increases the available number of Pt sites by a factor of 2, UV cleaning is much more effective in removing PVP, increasing the number of available Pt sites by a factor of 10. This may also explain the instability of UV-cleaned nanoparticles during reaction compared to solvent-cleaned nanoparticles. It appears that solvent-cleaned nanoparticles are stabilized by a significant amount of PVP that covers more than half of the nanoparticle surface.

4. CONCLUSIONS

Two major challenges of observing catalytic reaction intermediates on ligand-capped nanoparticles were addressed

in this study — interference by the organic capping agent in the SFG signal and blocking of active sites. Under hydrogenation reaction conditions, the capping agent (PVP) undergoes disordering on Pt, resulting in negligible SFG signal from PVP in the C−H stretch range. This is significant because it provides a clean background for probing reaction intermediates with SFG vibrational spectroscopy. Solvent cleaning removes PVP and increases the number of Pt active sites. This enhances catalytic activity and allows reaction intermediates to be observed with SFG. Although a larger increase in catalytic activity can be obtained with UV cleaning, this method results in aggregation of nanoparticles during reaction at temperatures as low as 373 K. However, solvent-cleaned nanoparticles demonstrate good stability up to at least 473 K. Accordingly, solvent cleaning is desirable when probing size and shape effects on nanoparticle catalysts, because it allows for SFG studies to be carried out without compromising size monodispersity under reaction conditions.

■ AUTHOR INFORMATION

Corresponding Author
*E-mail: lrbaker@lbl.gov (L.R.B.). E-mail: somorjai@berkeley.edu; Tel: 510-642-4053; Fax: 510-643-9668 (G.A.S.).

Notes
The authors declare no competing financial interest.

■ REFERENCES

(1) Shen, Y. R. *Nature* **1989**, *337*, 519.
(2) Lambert, A. G.; Davies, P. B.; Neivandt, D. J. *Appl. Spectrosc. Rev.* **2005**, *40*, 103.
(3) Kliewer, C. J.; Bieri, M.; Somorjai, G. A. *J. Am. Chem. Soc.* **2009**, *131*, 9958.
(4) Yang, M.; Somorjai, G. A. *J. Am. Chem. Soc.* **2004**, *126*, 7698.
(5) Yang, M.; Chou, K. C.; Somorjai, G. A. *J. Phys. Chem. B* **2003**, *107*, 5267.
(6) Bratlie, K. M.; Komvopoulos, K.; Somorjai, G. A. *J. Phys. Chem. C* **2008**, *112*, 11865.
(7) Kliewer, C. J.; Aliaga, C.; Bieri, M.; Huang, W.; Tsung, C.-K.; Wood, J. B.; Komvopoulos, K.; Somorjai, G. A. *J. Am. Chem. Soc.* **2010**, *132*, 13088.
(8) Bratlie, K. M.; Lee, H.; Komvopoulos, K.; Yang, P.; Somorjai, G. A. *Nano Lett.* **2007**, *7*, 3097.
(9) Kuhn, J. N.; Huang, W.; Tsung, C.-K.; Zhang, Y.; Somorjai, G. A. *J. Am. Chem. Soc.* **2008**, *130*, 14026.
(10) Somorjai, G. A.; Park, J. Y. *J. Chem. Phys.* **2008**, *128*, 182504.
(11) Lee, I.; Delbecq, F.; Morales, R.; Albiter, M. A.; Zaera, F. *Nat. Mater.* **2009**, *8*, 132.
(12) Narayanan, R.; El-Sayed, M. A. *Nano Lett.* **2004**, *4*, 1343.
(13) Borodko, Y.; Humphrey, S. M.; Tilley, T. D.; Frei, H.; Somorjai, G. A. *J. Phys. Chem. C* **2007**, *111*, 6288.
(14) Ullah, M. H.; Chung, W. S.; Kim, I.; Ha, C. S. *Small* **2006**, *2*, 870.
(15) Kim, J.; Chou, K. C.; Somorjai, G. A. *J. Phys. Chem. B* **2003**, *107*, 1592.
(16) Ramirez, E.; Eradès, L.; Philippot, K.; Lecante, P.; Chaudret, B. *Adv. Funct. Mater.* **2007**, *17*, 2219.
(17) Zheng, H.; Smith, R. K.; Jun, Y.-W.; Kisielowski, C.; Dahmen, U.; Alivisatos, A. P. *Science* **2009**, *324*, 1309.

(18) Aliaga, C.; Park, J. Y.; Yamada, Y.; Lee, H. S.; Tsung, C. K.; Yang, P. D.; Somorjai, G. A. *J. Phys. Chem. C* **2009**, *113*, 6150.

(19) Vidal-Iglesias, F. J.; Solla-Gullón, J.; Herrero, E.; Montiel, V.; Aldaz, A.; Feliu, J. M. *Electrochem. Commun.* **2011**, *13*, 502.

(20) Su, X. C.; Kung, K.; Lahtinen, J.; Shen, R. Y.; Somorjai, G. A. *Catal. Lett.* **1998**, *54*, 9.

(21) Su, X. C.; Kung, K. Y.; Lahtinen, J.; Shen, Y. R.; Somorjai, G. A. *J. Mol. Catal A: Chem.* **1999**, *141*, 9.

(22) McCrea, K. R.; Somorjai, G. A. *J. Mol. Catal A: Chem.* **2000**, *163*, 43.

(23) Yang, M.; Somorjai, G. A. *J. Phys. Chem. B* **2004**, *108*, 4405.

(24) Yang, M. C.; Chou, K. C.; Somorjai, G. A. *J. Phys. Chem. B* **2004**, *108*, 14766.

(25) Manner, W. L.; Girolami, G. S.; Nuzzo, R.G. *J. Phys. Chem. B* **1998**, *102*, 10295.

(26) Kuhn, J. N.; Tsung, C.-K.; Huang, W.; Somorjai, G. A. *J. Catal.* **2009**, *265*, 209.

(27) Rioux, R. M.; Song, H.; Hoefelmeyer, J. D.; Yang, P.; Somorjai, G. A. *J. Phys. Chem. B* **2005**, *109*, 2192.

(28) Song, H.; Kim, F.; Connor, S.; Somorjai, G. A.; Yang, P. D. *J. Phys. Chem. B* **2005**, *109*, 188.

(29) Kweskin, S. J.; Rioux, R. M.; Habas, S. E.; Komvopoulos, K.; Yang, P.; Somorjai, G. A. *J. Phys. Chem. B* **2006**, *110*, 15920.

(30) Curtis, A. D.; Burt, S. R.; Calchera, A. R.; Patterson, J. E. *J. Phys. Chem. C* **2011**, *115*, 11550.

(31) Borodko, Y.; Habas, S. E.; Koebel, M.; Yang, P. D.; Frei, H.; Somorjai, G. A. *J. Phys. Chem. B* **2006**, *110*, 23052.

(32) Rumpel, A.; Novak, M.; Walter, J.; Braunschweig, B.; Halik, M.; Peukert, W. *Langmuir* **2011**, *27*, 15016.

(33) Perry, D. A.; Hemminger, J. C. *J. Am. Chem. Soc.* **2000**, *122*, 8079.

(34) Hirschl, R.; Delbecq, F.; Sautet, P.; Hafner, J. *J. Catal.* **2003**, *217*, 354.

(35) Vig, J. R. *J. Vac. Sci. Technol. A* **1985**, *3*, 1027.

17546

dx.doi.org/10.1021/jp303363m | *J. Phys. Chem. C* 2012, 116, 17540−17546